Circle fixation from edge points

Daniel M. Topa
WaveFront Sciences, Inc.
14810 Central Ave. SE, Albuquerque, NM 87123-3905
dtopa@wavefrontsciences.com

We describe three methods for finding the origin and radius of a circle from a sample of points near the edge. This analysis assumes that the edge points are uniformly distributed about some constant radius *r*.

1. Problem formulation and three methods

Consider a circular lamina demarcated by a series of *n* points lying very near the edge. We may consider that the points were exactly on the edge and then perturbed along the radius by some random process. How might we use these perturbed points to determine the radius and origin of the circle?

The first method to consider is a simplistic attempt which starts with the trial function for a circle with origin $O^T = (x_0, y_0)$ and radius *r*

$$(x_i - x_0)^2 + (y_i - y_0)^2 = r^2 . \tag{1}$$

and attempts to minimize

$$\chi^2(r, x_0, y_0) = \sum_{i=1}^{n} (r^2 - (x_i - x_0)^2 - (y_i - y_0)^2)^2 . \tag{2}$$

The problem is that the fitting parameters, *r* and (x_0, y_0), are non-linear in this formulation. Certainly, this is soluble, but we are strongly motivated to look for a proper linear formulation.

First, it is more convenient to express these formulations in a vector form. Consider an arbitrary vector *p*

$$p = (p_0, p_1) \tag{3}$$

where the indices 0 and 1 can be mapped to a Cartesian coordinate system. Here, the points *p* will be the locations of the measured edge points. This allows equation 1 to be recast as

$$\|r_i\|^2 = r^2 \tag{4}$$

where

$$r_i \equiv p_i - O \tag{5}$$

and $\|r_i\|$ stands for the L2 norm of the vector r_i, that is $\|r_i\|^2 = r_i^T \cdot r_i$. In this notation the merit function takes the form

$$\chi^2(O) = \sum_{i=1}^{n} (r^2 - r_i^T \cdot r_i)^2 \tag{6}$$

After examining the problem in this notation, a second method presents itself. This method uses differences between measurements. Consider the difference between different measurements *i* and *j*:

$$r_i^T \cdot r_i = r^2 ,$$

$$r_j^T \cdot r_j = r^2 .$$

We can eliminate the variable *r* through subtraction to get

$$\Delta_{ij}^T \cdot O = \frac{1}{2}(p_i^T \cdot p_i - p_j^T \cdot p_j) \tag{7}$$

where the difference quantity is defined as

$$\Delta_{ij}^T \equiv p_i - p_j . \tag{8}$$

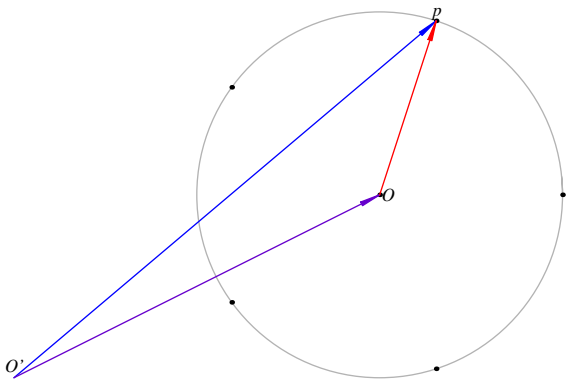

Figure 1: The radius vector. The three points of interest are the origin of the coordinate system *O'*, the center of the circular lamina *O* and the measured point *p*. We are interested in minimizing the sum of the magnitudes of the radius vectors. The radius vector in red is the difference between the local origin vector in purple and the measured vector in blue.

It is helpful to define the scalar quantity

$$\alpha_{ij} \equiv \frac{1}{2}(p_i^T \cdot p_i - p_j^T \cdot p_j) \,, \tag{9}$$

Equation 7 serves as the foundation for a linear least squares fit. We may pose the linear minimization problem in the notation of P. Riera

$$\chi^2(O) = \sum_{i=1}^{n-1} \sum_{j=i+1}^{n} (\Delta_{ij}^T \cdot O - \alpha_{ij})^2 \,. \tag{10}$$

where we are now summing over the $n(n+1)/2$ pairs of points. The fitting parameters in O are now presented in a linear form and therefore we will have a direct solution. The radius parameter r is missing, and will be computed from using equation 1 and the origin derived from the minimization of equation 10.

Interestingly enough, the difference method has caused the r parameter to disappear. We are now solving for the circle origin only. After the origin is computed, we can use equation 1 to generate a list of n values for r_i. The reported average and uncertainty for the radius are the average and standard deviation of this list.

The third and final approach we will consider is one where we minimize the size of the radius vectors. Consider figure 1. The point *O'* represents the origin of some coordinate system and *O* is the center of the circular lamina under consideration. An arbitrary measurement point is labelled as *p*. From examining the figure we can write

$$r = O - p \tag{11}$$

and we can formulate a merit function which minimizes the sum of the squares of the magnitudes of the n radius vector. It is

$$\chi^2(O) = \sum_{i=1}^{n} (r_i^T \cdot r_i)^2 \tag{12}$$

There is a close relationship between this and equation 6. While one may expect them to yield the same solution, we sill find subtle differences.

Inspecting this merit function shows that the fitting parameters, O, are not linear. However this instance represents a special case and we will be able to find a direct solution.

2. Simulation and results

To study the accuracy and precision of the three different minimization schemes presented in equations 6, 10 and 12, model data was created. Because the input data is known to arbitrary precision, we are able to make extremely precise quantizations of the performance of technique. We are able also to characterize the breakdown of the methods in low-sample and high-noise data sets.

Modelling is an essential step in algorithm development. For it not only provides a framework for quantification of performance, it also serves to validate the computer code. Typically known or special cases are studied and if the model deviates from the expected performance, we may have an error in the algorithm or the implementation.

2.1 Simulation method

The basic strategy was to select a fixed origin O and radius r. The linear sample density was varied from as few as three points on the edge to tens of thousands. The sample points were equally spaced in terms of angular distribution. Each edge point was perturbed radially. The perturbations were uniformly distributed with a fixed standard deviation. The set of perturbed points was an input for each of the three methods.

The arbiter of accuracy was the magnitude of the error in the computed position of the origin. For an input origin O, we compute a measured origin Q and an error vector $\varepsilon \equiv O - Q$. For plotting purposes, it is convenient to condense the error vector down into a single number. The key is to realize the significance of the error vector. It describes an ellipse which should hold about half of the measurements. Or we may think of it as the ellipse which has a fifty percent probability of containing successive measurements. Since this ellipse becomes more circular with improved statistics, we may as the a natural question what circle has the same area as the ellipse. Consider an ellipse of semi-major axis a and semi-major axis b. What size circle will have the same area as the ellipse? In mathematical terms, what is r in

$$\pi r^2 = \pi ab \,? \tag{13}$$

The solution is $r = \sqrt{ab}$ where neither a nor b has a sign. To connect back to the error vector, we will characterize the vector with one number

$$e = \sqrt{\varepsilon_0 \varepsilon_1}\,. \tag{14}$$

A secondary quality measure involved the radius. But in this instance it is not appropriate to compare a measured radius to the input radius ρ. For the input radius is a goal; what the data create are an effective radius r. We may clarify this issue by discussing the model data in more detail. We start with three inputs: the point O and the radius ρ. We have a linear sample density of n points distributed evenly over 2π radians. This generates a point every $\Delta = 2\pi/n$ radians. The radius is then perturbed using a normal distribution $P(\rho)$

$$P(\rho;\rho_0,\sigma) = \frac{1}{\sigma\sqrt{2\pi}} Exp(-(\rho-\rho_0)^2/2\sigma^2) \tag{15}$$

where we have explicitly shown the parameters ρ_0 and σ in the function P. For example at the ith point, the angle is $\theta_i = i\Delta$ and the radius is

$$r_i = \rho + \delta\rho_i \tag{16}$$

where $\delta\rho_i$ is chosen from the distribution $P(\rho;0,\sigma)$. The perturbed edge point becomes

$$p_i = r_i \begin{bmatrix} \cos\theta_i \\ \sin\theta_i \end{bmatrix} + O\,. \tag{17}$$

In this formulation it is apparent that the radius of interest is not the input radius ρ, but the effective radius $\bar{r}$ of the ensemble defined as the average of all the perturbed radii;

$$\bar{r} = \left(\sum_{i=1}^{n} r_i \right) / n\,. \tag{18}$$

We see from equation 5 that this r value is a vector. We can express equation 18 in a scalar form as

$$\bar{r} = \left(\sum_{i=1}^{n} \|r_i\| \right) / n\,. \tag{19}$$

The radius error then becomes the difference between the effective radius $\bar{r}$ and the measured effective radius r_i.

But the output of these algorithms is an origin, not a radius, so we must evaluate the computation of the origin. Since we are using ideal data, we can quantify the accuracy of the calculation as the difference between the input origin O and the measured origin O. The precision and accuracy of each method will be quantified in section 3.

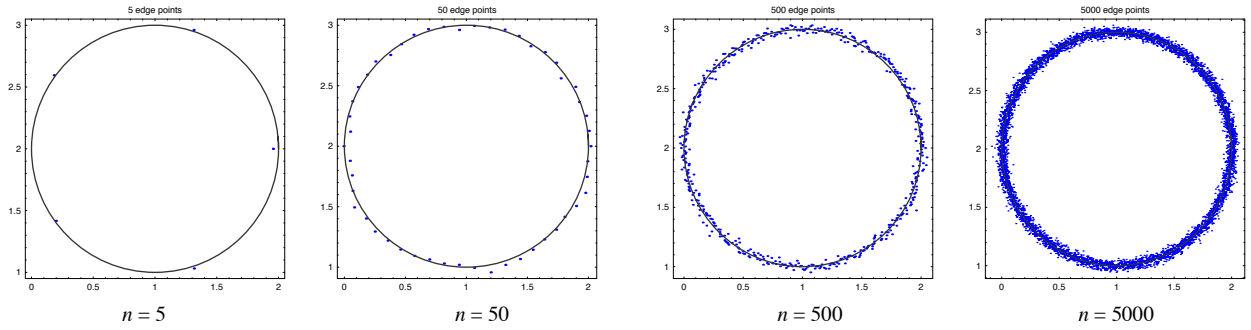

Figure 2: The data sets used in table 1. Different sets of points were used. The first figure shows 5 points, the subsequent figures show 50, 500 and 5000 points successively. The blue dots represent perturbed edge points; the circle shows the input solution. As shown in the table, the accuracy continues to improve as we add additional points.

Later on we will see a need to sweep through the data set again to compute statistical information. For large data sets this can double the run time. To preclude this wasteful step, we must collect certain sums as the data is generated. Start by defining the quantity *P,* a vector of vectors

$$P^T = \sum_{i=1}^{n} [p_i, p_i^2, p_i^3, p_i^4] \tag{20}$$

and the 2×2 matrix of scalars M

$$M_{\alpha\beta} = \sum_{i=1}^{n} p_{i_0}^{\alpha} p_{i_1}^{\beta} . \tag{21}$$

Also, as the radius values are being created using equation 16, it is prudent to collect R the average of scalars

$$R = n^{-1} \sum_{i=1}^{n} [r_i, r_i^2, r_i^4] . \tag{22}$$

2.2 Simulation results

The results of several runs were used to evaluate the methods. For these runs, the following values where used:

$$O^T = \begin{bmatrix} 1 & 2 \end{bmatrix}, r = 1, \text{and } \sigma = 0.025 .$$

A series of runs were made with n points, where the values of n used were 5, 50, 500, and 5000 as depicted in figure 2. The numerical results are summarized in table 1 below. The data in this table help to establish a few important conclusions.

The first is that the minimization problems presented in equations 6 and 10 are equivalent in that they return the same origins. While there are differences in the sixth or seventh decimal place, these differences are too small to affect a physical measurement. Interestingly enough, the radius computation is consistently better, especially so for the larger point sets. The second conclusion is that while the solutions to the minimization problems in equations 10 and 12 are similar, the accuracy of the latter is superior.

An important result is that we can abandon formulating an iterative solution for equation 6; the direct solution for the minimization of equation 10 is much faster and offers equivalent origin location accuracy and improved radius accuracy.

3. Direct solutions

All linear least square fits offer a direct solution. In general, a direct solution is preferable to an iterative solution. The iterative solutions propagate error and sometimes involve complicated schemes to locate the minimum. In some case, iterative methods may return a local minimum instead of the global minimum being sought. So while the process of minimizing equation 6 is elementary, we still searched for a direct solution in the interest of reducing computation time. The iterative problem generates a slightly better solution as we might expect since it has an extra degree of freedom. But the improvement appears in the fourth to sixth decimal place. This means the improvement is too fine to be realized in a practical measurement.

	eqn 6	eqn 10	eqn 12	eqn 6	eqn 10	eqn 12
n	origin accuracy	origin accuracy	origin accuracy	radius accuracy	radius accuracy	radius accuracy
5	5.0 E-3	5.0 E-3	4.2 E-3	-2.2 E-4	5.9 E-5	4.0 E-5
50	6.2 E-3	6.2 E-3	3.2 E-3	-2.3 E-4	2.2 E-5	1.1 E-4
500	2.5 E-3	2.5 E-3	2.0 E-3	-2.9 E-4	4.0 E-6	2.6 E-6
5000	4.0 E-4	4.0 E-4	3.8 E-4	-3.1 E-4	8.1 E-8	7.4 E-8

Table 1: Numerical comparison of three fitting methods.

When we turn our attention to the minimization of equation 12, we are able to exploit the conjugate variables and formulate a direct solution here too. So iteration is not needed. This means that minimization of equations 10 and 12 is a direct process and both methods will deliver a full precision solution much faster.

On topic left unexplored is the difference between the problems presented in equations 10 and 12. They appear to be the same problem, differing only by a constant offset.

3.1 Minimizing the differences between measurements

The minimization problem presented by equation 10 has an elementary solution. We follow the canonical approach by requiring that the derivatives with respect to the fitting parameters be zero simultaneously. That is,

$$\partial_\mu \chi^2 = \sum_{i=1}^{n-1} \sum_{j=i+1}^{n} (\Delta_{ij}^T \cdot O - \alpha_{ij})(\Delta_{ij})_\mu = 0 , \tag{23}$$

where μ is the spatial index and

$$\partial_\mu = \frac{\partial}{\partial x_\mu} \tag{24}$$

represents the derivative with respect to the μth coordinate of the target vector x. For a physical space of N dimensions, equation 23 represents N separate equations linear with respect to the fitting parameters. These equations are best expressed in a matrix notation. For example,

$$A \cdot O = B . \tag{25}$$

For the two-dimensional space of the circular lamina, the matrix A takes the form

$$A_{\mu\nu} = \sum_{i=1}^{n-1} \sum_{j=i+1}^{n} (\Delta_{ij})_\mu (\Delta_{ij})_\nu . \tag{26}$$

and the vector B becomes

$$B_\mu = \sum_{i=1}^{n-1} \sum_{j=i+1}^{n} \alpha_{ij} (\Delta_{ij})_\mu . \tag{27}$$

The solution O is then

$$O = A^{-1} \cdot B . \tag{28}$$

Noting that the inverse (*e.g.* [1], p. 81) of a square non-singular matrix M is given by

$$M^{-1} = \frac{adj(M)}{det(M)} \tag{29}$$

where *adj(M)* is the adjoint matrix, the transpose of the cofactor matrix, we can formulate the solution to a system like equations 26 and 27. Using the shorthand notation

$$A = \begin{bmatrix} a & b \\ b & c \end{bmatrix}, \text{and } B = \frac{1}{2}\begin{bmatrix} u \\ d \end{bmatrix} \tag{30}$$

the inverse is

$$A^{-1} = \frac{1}{\Delta}\begin{bmatrix} c & -b \\ -b & a \end{bmatrix} \tag{31}$$

and the solution becomes

$$O = \frac{1}{2\Delta}\begin{bmatrix} cu - bd \\ ad - bu \end{bmatrix}, \tag{32}$$

where the determinant Δ is

$$\Delta = ac - b^2 . \tag{33}$$

To express the answer and the uncertainty we will need some common summations. We will retain the scalar definition

$$b = \sum_{i=1}^{n-1} \sum_{j=i+1}^{n} (\Delta_{ij})_0 (\Delta_{ij})_1 \tag{34}$$

and add two new vector variables

$$a = \sum_{i=1}^{n-1} \sum_{j=i+1}^{n} \Delta_{ij}^2 , \text{and } c = \sum_{i=1}^{n-1} \sum_{j=i+1}^{n} \alpha_{ij}\Delta_{ij} \tag{35}$$

and a new scalar definition

$$d = \sum_{i=1}^{n-1} \sum_{j=i+1}^{n} \alpha_{ij}^2 . \tag{36}$$

We can now recast the solution in equation 32 in vector form as

$$O_\mu = \frac{1}{2\Delta}(a_\nu c_\mu - b c_\nu) \tag{37}$$

where ν is the coordinate orthogonal to μ $(\nu = 2 - \mu)$ and the determinant is now

$$\Delta = a_0 a_1 - b^2 . \tag{38}$$

The fundamental pieces that compose the intermediate quantities are $(p_i)_\mu - (p_j)_\mu$ and $(p_i)_\mu^2 - (p_j)_\mu^2$.

With the origin now available, we may measure an effective radius defined by this point

$$\overline{r_m} = \left(\sum_{i=1}^{n} \| p_i - O \| \right) / n . \tag{39}$$

The uncertainty in this term is defined in the standard way

$$\sigma_{\overline{r_m}} = \sqrt{\overline{r_m^2} - \overline{r_m}^2} . \tag{40}$$

The evaluation of the precision in the origin is a bit more involved. We start by expressing the merit function in terms of the intermediate variables in equations 34-36. The χ^2 function now becomes

$$\chi^2(O) = d + 2bO_0O_1 + \sum_{\mu=0}^{1} O_\mu(O_\mu a_\mu - c_\mu) \tag{41}$$

Equation 41 is a a vital element in the error analysis because it used to form s^2, the sample variance for the fit ([2], pp. 137, 154):

$$s^2 = \frac{\chi^2}{n-3}. \tag{42}$$

From this, we can estimate the errors in the fitting parameters using the method derived in [2], p. 245. The general solution is

$$\sigma_\mu^2 = s^2 \frac{2}{\partial_\mu^2 \chi^2}. \tag{43}$$

Now we reap an additional benefit of the new formulation of χ^2 because it is trivial to evaluate the second derivative

$$\partial_\mu^2 \chi^2 = 2a_\mu \tag{44}$$

and get the final solution

$$\sigma = \sqrt{\frac{s^2}{a}}. \tag{45}$$

Since we have created the input data, we have the information that we need to measure the accuracy of the answers. These quantities are

$$\text{origin accuracy} = q - O \text{, and radius accuracy} = \bar{r} - \bar{r}_m. \tag{46}$$

Notice that the radius accuracy uses the effective radius $\bar{r}$ instead of the input radius ρ.

Consideration of the residuals requires some thought. In a general sense, a least squares fit in minimizing the square of the difference between a measured dependant variable like y_i and a trial function of an independent variable, $y(x_i)$. So every point should have a corresponding residual value like $y_i - y(x_i)$. How then do we apply this prescription to the problem at hand? After all, the output is a point, consisting of two numbers - the origin. We must resolve the relationship between the origin O and the input points p.

The relationship of course is through the effective radius. This may appear to conflict the methodology of the fit since we deliberately contrived a method to eliminate the explicit calculation of the radius. While the radius was not explicit, it was certainly implicit. The trial function we are resolving is a circular function specified by an origin and a radius. With this realization we can then compute the implied radius at each point p using the computed origin O. The residual value we see plotted in the right-hand side of figure 4 is the difference between the square of the measured radius and the square of $\bar{r}_m$.

3.2 A correlation measure for the circle

In this section we present of the correlation index r_c^2 [4]. We will define a circular correlation index and use it to evaluate both methods. Since these methods are based on computing r^2 in lieu of r, the definition we will use

$$r_c^2 = 1 - \frac{SSE}{s_{r^2}^2} \tag{47}$$

where SSE the sum of the squares of the errors and the sum of the r^2 are

$$SSE \equiv \sum_{i=1}^{n} (r_i^2 - \hat{r}_i^2), \; s_{r^2}^2 \equiv \sum_{i=1}^{n} r_i^2. \tag{48}$$

In this notation r_i^2 is the measured value (the square of the magnitude of equation 5) and $\hat{r}_i^2$ is the square of the predicted value.

After computing the origin (in this case via equation 37), we compute the R vector using equation 22. Note that R_0 is the measured effective radius $\bar{r}_m$. The correlation index can now be expressed as

$$r_c^2 = 1 - \frac{R_0^2(R_0^2 - 2R_1) + R_2}{R_1}. \tag{49}$$

Figure 3 shows an example of data sets with varying scatter and the corresponding correlations. The correlation index describes how well the data correlates to a circle. You might think of this as describing how likely the ordinate is to change as the abscissa varies.

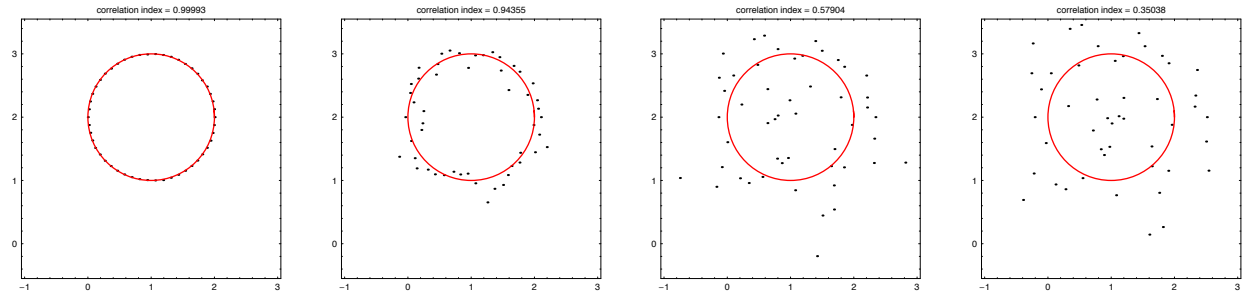

$r_c^2 = 0.99993$ $r_c^2 = 0.94$ $r_c^2 = 0.58$ $r_c^2 = 0.35$

Figure 3: A graphic example showing data quality and the correlation index. In this example, we start with high-quality (low-noise) data on the left and increase the noise as we move to the right. The correlation index is a critical parameter; the least squares fit will always return an answer as shown above. The correlation index gives us an important clue regarding the quality of the data and the applicability of the model. However one should also closely inspect the uncertainties in the origin and radius too.

3.3 Minimizing the radius vectors

We now turn to the very interesting minimization problem in equation 12. Clearly the fitting parameters O are non-linear. For emphasis we can recast the merit function as

$$\chi^2(x_0, y_0) = \sum_{i=1}^{n} \left((x_i - x_0)^2 + (y_i - y_0)^2\right)^2 . \tag{50}$$

This seems to preclude a direct solution. However, we are saved by the facts that the fitting parameters O are conjugate and quadratic. With conjugate parameters, we are able to solve for x_0 and y_0 separately. The frees us from an iterative solution that improves one variable at the expense of the other. And because the variables are quadratic, the method of inverse parabolic interpolation ([3], p. 395, [2], p. 209) yields an exact solution.

Inverse parabolic interpolation is the process that takes three points on a parabola and computes the abscissa of the minimum. The process is used to approximate some solutions since many minima have a parabolic behavior in some neighborhood of the minimum. In this case, the minimum is exactly parabolic and the location of the minimum will be exact.We present here a different form and derivation that the previously cited sources. Begin with a generic quadratic function

$$y(x) = d_0 + d_1 x + d_2 x^2 . \tag{51}$$

The extremum of this function is the point where the derivative is zero; *i.e.* $y' = 0$.
So the extremum depends only upon the two higher order coefficients

$$x_{min} = -\frac{d_1}{2d_2} . \tag{52}$$

It turns out that we only need three points to determine the ratio in equation 52. Consider three arbitrarily chosen points, $(a, y(a))$, $(b, y(b))$, $(c, y(c))$. Since we only need the ratio of the higher order coefficients, an immediate goal is to remove the constant term, and this is quickly accomplished via subtraction:

$$y(b) - y(c) = d_1(b - c) + d_2(b^2 - c^2) ,$$

$$y(b) - y(a) = d_1(b - a) + d_2(b^2 - a^2) .$$

We are left with an elementary linear system

$$\begin{bmatrix} (b-c) & (b^2-c^2) \\ (b-a) & (b^2-a^2) \end{bmatrix} \begin{bmatrix} d_1 \\ d_2 \end{bmatrix} = \begin{bmatrix} y(b)-y(c) \\ y(b)-y(a) \end{bmatrix} \tag{53}$$

and when we solve for d_1 and d_2 and put these values back into equation 52 we get

$$x_{min} = \frac{1}{2}\frac{a^2(y(b)-y(c)) + b^2(y(a)-y(c)) + c^2(y(b)-y(a))}{a(y(b)-y(c)) + b(y(c)-y(a)) + c(y(a)-y(c))} . \tag{54}$$

Another solution is given in [3] (equation 10.2.1, p. 395):

$$x_{min} = b - \frac{1}{2}\frac{(b-a)^2[y(b)-y(c)] - (b-c)^2[y(b)-y(a)]}{(b-a)[y(b)-y(c)] - (b-c)[y(b)-y(a)]} . \tag{55}$$

Finally, we cite the form given in [2] (equation 11-4, p. 210)

$$x_{min} = c - (b-a)\left[\frac{y(c)-y(b)}{y(c)-2y(b)+y(a)} + \frac{1}{2}\right] . \tag{56}$$

The strategy of the fit is straightforward. First we find the abscissa of the minimum, then we find the ordinate of the minimum. One suggested method is to use the extreme points of the data set. For example, the first three points would be

$$(x_{min}, \chi^2(x_{min}, y_{mid})) , (x_{mid}, \chi^2(x_{mid}, y_{mid})) , \text{and } (x_{max}, \chi^2(x_{max}, y_{mid})) \tag{57}$$

where the subscript *mid* denotes a midpoint, *e.g.*,

$$x_{mid} = \frac{1}{2}(x_{min} + x_{max}) , \tag{58}$$

and the χ^2 function is defined in equation 12. Hopefully these extreme points can be captured in the routine that identifies edge points. In the interest of clarity, we list the three points needed to isolate the ordinate of the minimum:

$$(y_{min}, \chi^2(x_{mid}, y_{min})) , (y_{mid}, \chi^2(x_{mid}, y_{mid})) , \text{and } (y_{max}, \chi^2(x_{mid}, y_{max})) . \tag{59}$$

Note the repetition of the term $\chi^2(x_{mid}, y_{min})$.

Now that we have found the solution - the point which minimizes the χ^2 function - we need to evaluate the statistical uncertainty in the answer. To do this, we will need to generalize the Bevington prescription used in the previous section.

We begin with a subtle distinction between the previous fitting strategy and the case here. In the previous fit, we needed the quantities *a* and *c* to compute the origin. The vector *a* was all that was needed to compute the uncertainty (equation 45). We did not have to sweep through the data set again to compute residuals.The difference here is we use the reverse parabolic interpolation to find the minimum of the merit function so there is no need to vector sums for this purpose. But we will need vector sums to quantify the uncertainty.

We can rewrite equation 42 as

$$s^2 = \frac{ssr}{n-3} \tag{60}$$

where *ssr* is the sum of the squared residuals. These residuals are again the difference between the measured points *p* and the computed circle. The change here is that we are not using the merit function χ^2 , but instead the quantity *ssr*. To be explicit we show

$$ssr = \sum_{i=1}^{n} (\bar{r}^2 - r_i^2)^2 . \tag{61}$$

This formulation while correct is inefficient for a computer code since it requires one loop to compute the average and yet another to compute the variance. The more efficient statement is

$$ssr = n(\bar{r}^4 - 2\bar{r}^2\overline{r^2} + \overline{r^4}) ; \tag{62}$$

or in terms of the *R* vector in equation 22

$$ssr = R_0^2(R_0^2 - 2R_1) + R_2 . \tag{63}$$

We still need to differentiate equation 12 twice to compute the errors. Direct and successive differentiations of the quartic equation lead us to

$$\partial_\mu^2\chi^2 = \zeta_\mu = 12(a_\mu + b_\mu + c_\mu) + 4(a_\nu + b_\nu + c_\nu) \tag{64}$$

where the intermediate quantities are

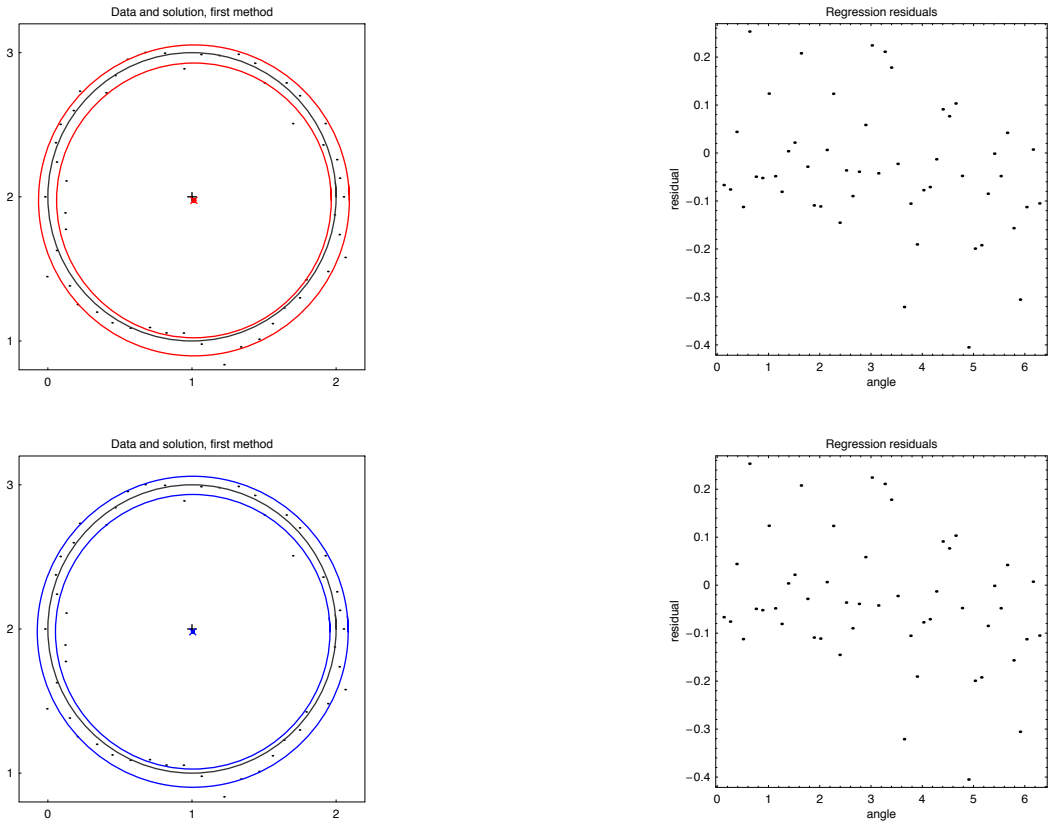

fit *residuals*

Figure 4: A sample fit to a common data set shows the differences between the two methods. The data and regression solutions are shown on the left; the residuals on the right. The black dots are the points p from equation 17. In both figures the black cross is the target origin O in equation 17. The black circle is plotted around this point with an effective radius $\bar{r}$ from equation 16. The colored crosses mark and small circles denote the computed origin. (For the first methods, equations 37 and 45, for the second, 54 and 66). The two large colored circles have radii of $\bar{r}_m \pm \sigma_r$. It is very important to check the residuals to verify a random pattern that would preclude most systematic errors. The standard deviation of the normally distributed noise was 0.075. Numeric values are presented in table 2.

$$a = \sum_{i=1}^{n} p_i^2 \ , \ b = 2O \sum_{i=1}^{n} p_i \ , \text{and } c = nO^2 \ . \tag{65}$$

Note that the quantities a and b can be harvested from the P vector in equation 20. At last the error in the origin is

$$\sigma = \sqrt{\frac{2ssr}{(n-3)\zeta}} \ . \tag{66}$$

.

	first method	second method
origin	(1.014, 1.975) ± (0.013, 0.013)	(1.005, 1.981) ± (0.0092, 0.0091)
origin accuracy	(-0.014, 0.025)	(-0.005, 0.019)
measured effective radius	1.016 ± 0.063	1.016 ± 0.063
radius accuracy	-0.00020	-0.000099
correlation index	0.985	0.985

Table 2: Comparing the results of two methods on a data set of 50 points with $\sigma = 0.075$. The effective radius is 1.016 ± 0.063.

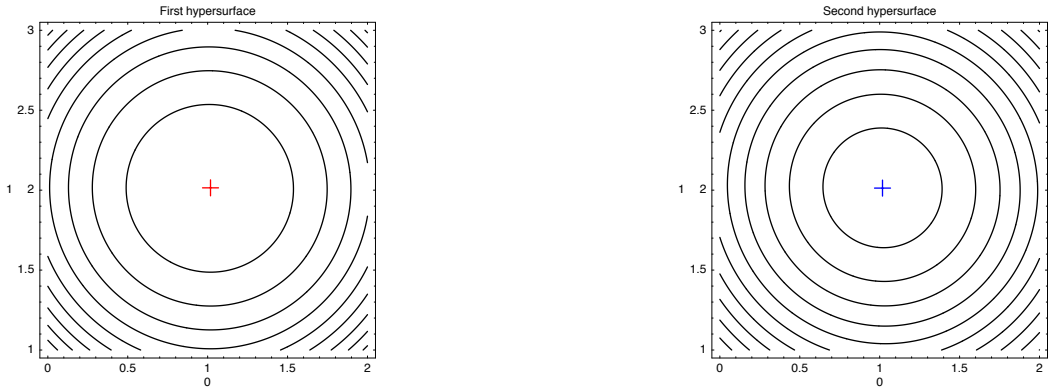

Figure 5: Solutions for both methods plotted against the parameter space hypersurface. Visual inspection affirms that each method has in fact found the true minimum. The first method is shown in *(a)* on the left; the second on the right in *(b)*. The labels 0 and 1 are the indices of the components of the origin O. We see that the second method has a steeper hypersurface. This leads us to expect a more precise solution.

As we shall see in section 4.2, we do have a way to validate these precision computations. To do this, we will take 500 sets of n data points and compute the average and standard deviation of the measured origins. This standard deviation of the meta-set origin should be comparable to the single episode precision.

Figure 4 and the companion table 2 show some typical results for the two methods. Although the measurements are basically comparable, we do see a small gain in precision and accuracy from the second method that is fairly consistent

We close this section with a more efficient method to compute the χ^2 function. In the previous method we needed to compute intermediate sums to calculate the uncertainties in the fitting parameters. Here there is no such need, we offer the more efficient form only as a method to reduce CPU time, especially for large data sets. As the data points are collected, we can build the summation quantities P and M (equations 20 and 21) rather inexpensively. We can then avoid having to sweep through the data again to compute the merit function in equation 50. Noting ν is the component conjugate to μ ($\nu = 1 - \mu$) the merit function is

$$\chi^2(O) = 2nO_0^2O_1^2 + 8M_{1,1}O_0O_1 + 2M_{2,2}$$

$$+ \sum_{\mu=1}^{2} P_{4,\mu} + O_\mu(O_\mu(nO_\mu^2 + 2P_{2,\nu} + 6P_{2,\mu} - 4P_{1,\mu}) - 4(P_{1,\mu}O_\nu^2 + P_{3,\mu} + M_{\mu,\nu})) \,. \tag{67}$$

4. Further comparisons

This section details the process used to verify that the theoretical development was correct and the results of different tests to evaluate the two methods. To do this we present several different computations to verify the behavior of the calculation. Most checks were qualitative; some we quantitative. Also, this section compares both methods using the criteria of speed, accuracy and precision and nominates a preferred method.

criterion	best method
speed	eq 12
accuracy	eq 12
precision	eq 12
pathological data	even

Table 3: Scorecard comparing the two methods

4.1 Summary

Table 3 presents a quick summary of the evaluations. The first difference that we note between these two methods is the amount of computation time needed. The first algorithm is $\Theta(n^2)$, whereas the second method is a much faster $\Theta(n)$. On small data sets the speed difference may be negligible, but for large data sets the difference can be dramatic.

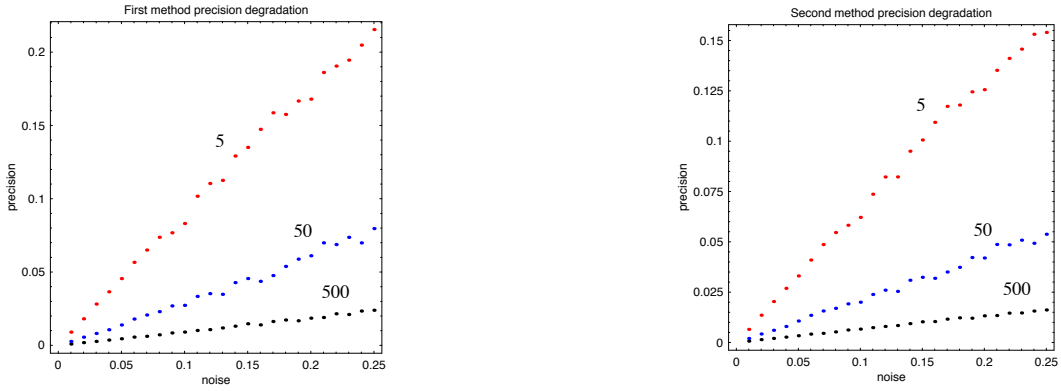

(a) *(b)*

Figure 6: Measurements showing precision degradation with increasing noise in the input. The first method is shown in *(a)* on the left; the second on the right in *(b)*. The independent axis is the input noise for the model, σ from equation 15. The dependant axis is the precision, computed on the left using equation 45 and on the right using equation 66. The red dots correspond to 5 points, the blue dots 50 points and the black dots 500 points.

The precision and accuracy improvements of the second method are modest, but definite. A more critical differentiation is in the run times, especially for large data sets (1000 points). For small data sets, the difference in runs times may not be distinguishable.

The performance with pathological data is interesting and difficult to characterize because the criteria are so subjective.The methods have very different performance in the individual tests. And so while the performance may be quantified, the relative value of the different tests is difficult to assess. Also, we found that the quality of the answer for the second method is dependant upon how uniformly the data is distributed. This tilts the scale in favor of the first method. However, the second method can be recast as a rapid iteration problem restoring the superior precision and accuracy of the second method. This tilts the scale in favor of the second method but leaves us with the dilemma of trying to quantify the trade-off between speed and precision.

4.2 Verification

The verification tests take two different forms. One is quantitative, the other qualitative. On the quantitative side, we are able to use repeated measurements to compute values calculated explicitly. For the qualitative case, we look for behavior trends. Then, after these tests are completed, we are ready to proceed with having the process expressed in C++ code. After that, we run a validation test. The computer code analyzes common sets of data and creates an output file. We then use *Mathematica* code to compare the C++ results to the *Mathematica* results and publish a report summary. So in this context verification is the process used to assure us that the theoretical development is reasonable and validation is the process used to insure that the computer code correctly implements the theory.

A simple first test is to plot the solution in parameters hyperspace. In this space, the origin point yields two dependent variables the height is given by the χ^2 function. This quick checks show whether or not the method has found a true minimum. Figure shows these plots for both methods. This figure also shows how the fit parameters are conjugate variables. This simple check usually verifies that the merit function has been posed and formulated properly.

The next step was a simple qualitative test. What we want to verify is that the precision of the computations decreases as the noise decreases, and that the models recover exact results when there is no noise at all. Figure 6 shows the results of this measurement. Qualitatively, the data behave as expected. The precision degrades as the noise increases. Also, measurements with more points do better that measurements with fewer points. And the errors shrink as the noise shrinks, allowing us to recover the exact answer when there is no noise at all. To check the case for no noise, we used an unperturbed data set eight points - a point every $\pi/4$ radians. This allows the symbolic capabilities of Mathematica to do an exact calculation and verify that the code behaved properly without noise. That is, the methods both recovered the solution exactly.

A series of measurements were made to search for the usual behavior in the precision. Typically in least squares fits, the computed precision has a trademark behavior best visualized in logarithmic space. Early on in the regime of few measurements, the precision improves rapidly giving way to a linear form as the number of measurements increases. This behavior was indeed manifest as shown in figure 8.

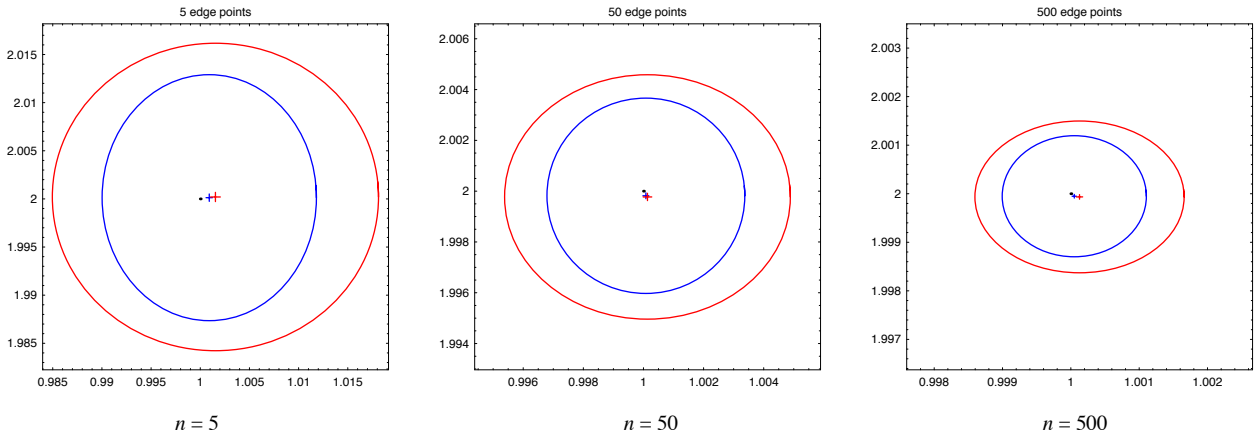

Figure 7: The measured precision of both methods. Cases for 5, 50 and 500 edge points were studied. Each case had 500 different data sets prepared and analyzed using both methods. The origin computations were then averaged to their values are marked with crosses - red for the first method, blue for the second. The ellipses around the crosses represent the standard deviation. This figure shows how the second method slightly more accurate and more precise. Numerical values are shown in table 4.

The next case involved actual measurements which are then compared to the computation. The process is simple. We generate 500 sets of n data points. For each set, we compute the origin using both methods. We then compute the average and standard deviation of the origins. These numbers then can be compared to the precision calculations.

A series of plots were prepared to help visualize these numbers and they are shown in figure 8. The computed precisions show the trademark shape in linear-log space. The precision rapidly improves in the regime of low n, but eventually assumes a linear behavior. The precision of the first method was computed using equations 45 and 14; the second method was computed using equations 66 and 14. Additionally we see that the second method consistently offers a modest improvement in precision. In summary, the computation passes this qualitative test.

Next, we tried to prepare a more quantitative test by actually measuring the precision and comparing this value to the computation. The first step was to prepare data series consisting of 500 measurements. This was done for $n = 5, 50, 500$. So for example, for $n = 5$, we prepared 500 different sets of five random points and the 500 origin values where then averaged.

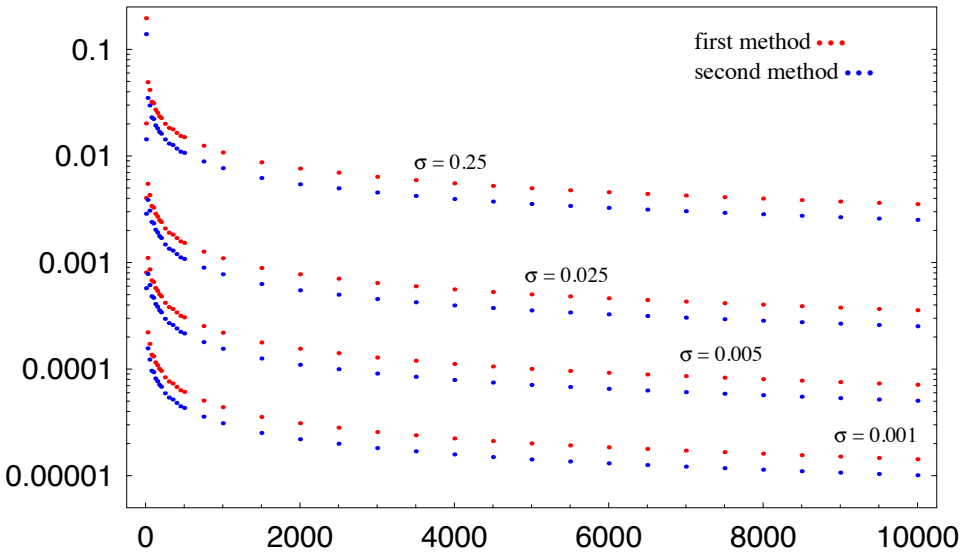

Figure 8: Precision improvement by increasing the number of measurements. The red dots mark the precision of the first method, as shown in equation 45. The blue dots are the precision of the second method as shown in equation 66. This is curve in linear-log space has the correct form so the computation passes this qualitative test.

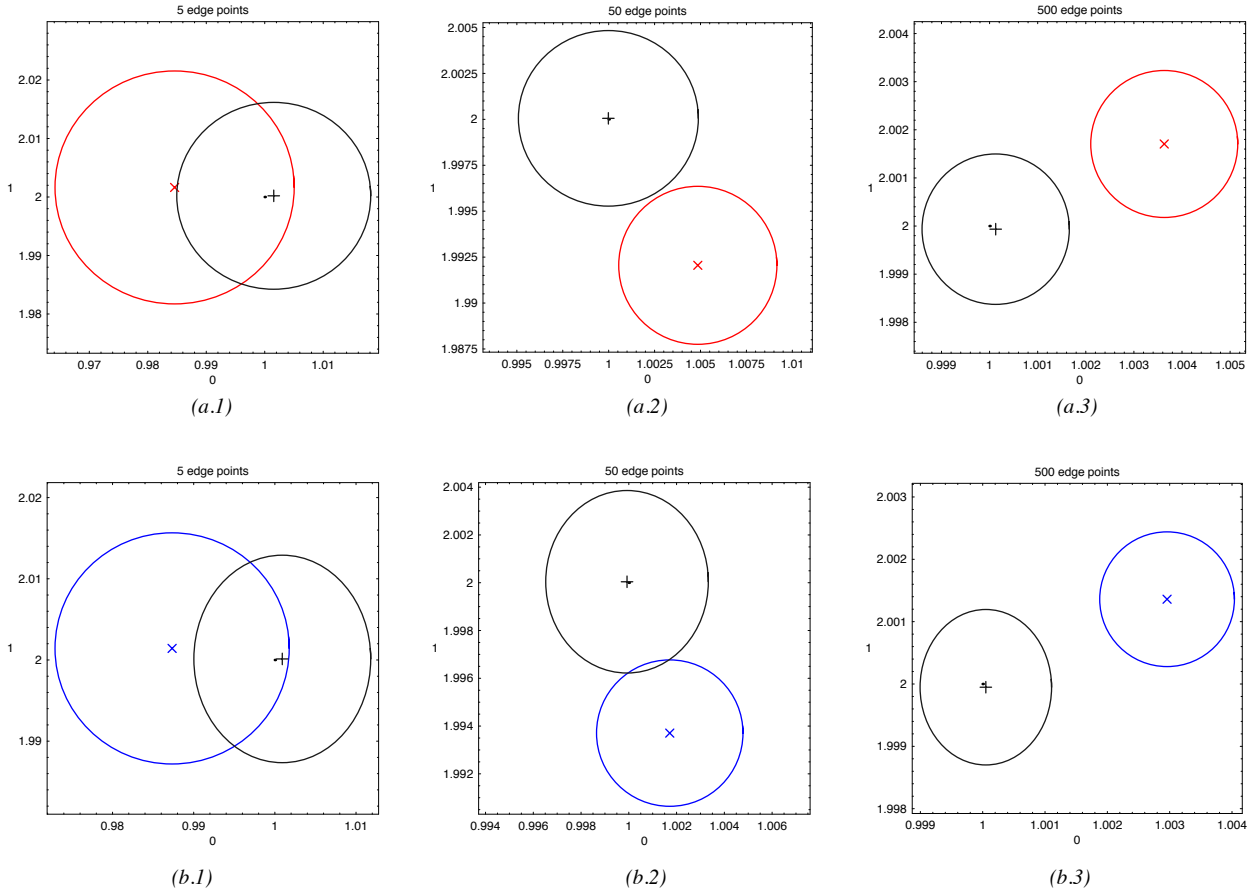

Figure 9: Measured precision vs. computed precision for an ensemble of 500 measurements with $\sigma = 0.025$. The center of the ellipse is the origin; the radii are the vectors $\bar{r}_m$ .The black ellipses represent the ensemble measurement. The colored circles, red for the first method (series *a*) and blue for the second (series *b*), are the results of a single measurement. The *.1 series is for $n = 5$, *.2 for $n = 50$, and *.3 for $n = 500$. We see that as the n grows the ellipses converge in size. These data are excerpted in table 4.

To plot these data, we used the vector standard deviations for the radii of the ellipses. These plots are shown in figure 7. Again, the black dot is the input origin q and the red curves represents the results from the first method, the blue curves, the second method. One nice feature of this presentation is that it instantly conveys the improved accuracy and precision of the second method. The precision is quantified by the size of the ellipse - smaller is better. The accuracy is quantified by how close the crosses are to the origin - the closer the better. Clearly, in all cases, the true answer lies within the error ellipse.

	5	50	500
single event origin error	0.021	0.0043	0.0015
ensemble origin error	0.016	0.0048	0.0015
single event origin error	0.014	0.0031	0.0011
ensemble origin error	0.012	0.0036	0.0011

Table 4: Precision computation vs. measurement for the data in figure 9. The input noise is $\sigma = 0.025$

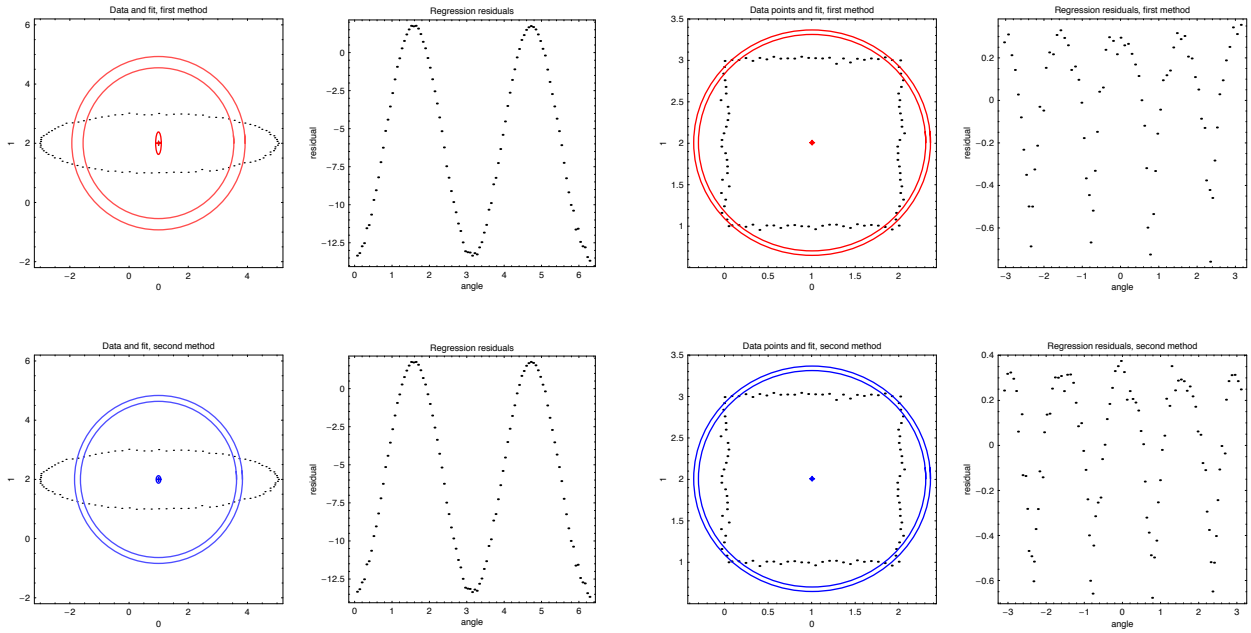

Figure 10: Pitfalls of correlated residuals. The four figures on the left show the results of fitting a circle to an elliptic data set; the four figures on the right to a square data set. The four figures on the top use the first method, the four figures on the bottom, the second method. For the fits, the two colored lines have radii of $\bar{r}_m \pm \sigma_{r_m}$. Clearly, a circle does not resemble a square of an ellipse and the correlated residuals indicate the trial function does not match the data. Notice in the figure in the upper right hand corner the first method suffers a more serious degradation in the origin precision. Also, these figures suggest that for symmetric data sets we have high centration accuracy.

The next test was the most qualitative. The purpose was to verify the improvement of the precision as the number of samples increases. Both methods were compared using different values of σ. The results are plotted in figure 8; note the precision is plotted on a logarithmic scale. The methods both had the characteristic shape: the precision rapidly improves and then the improvement becomes linear on the logarithmic scale. Also, the variation in σ had the desired effect separating the curves.

The precision computations are difficult to validate. The easiest probes of the correctness of the formulation come from behavior in the limits. For example, in the simple case of a single computation the precision may be off by a factor of 0.8 and it is nearly impossible to catch this. So we turn to behavior in the limits. We have already seen in figure 6 that the precision approaches zero as the input noise is decreased. This is not a rigorous test since the slopes allow for some variation, but it does reinforce our belief. Another test in the limit is a bit more quantitative. The goal is to take a few data sets ($n = 5, 50, 500$) and create 500 different data sets of n points. As the number of different data sets grows, the standard deviation of the 500 data sets must approach the precision predicted for a single data set. The convergence happens faster for higher n. Figure and table 4 show exactly these results. So we can say that in the large n limit, the precision is correct to at least two decimals.

4.3 Pathologies

A very interesting line of thought was initiated by P. Riera. He asked for quantification of problems with pathological data, for example a small clustering of points in lieu of the uniform distributions here. Or perhaps a non-circular data set. We are trying to make some crucial distinctions. First of all, what are the symptoms of a pathological regression. What should we look for in the results to see if the data is “reasonable”? And secondly, what happens to the accuracy of the calculations? Hopefully, this section reinforces the utility and interplay of the concepts of accuracy, precision and correlation.

4.3.1 Correlated residuals

We begin with a look at non-circular data sets. In order to be able to measure the accuracy, we used simple functions to create the input data. This allows us to quickly compare the measured origin to the input origin. The two functions used were an ellipse and a square. The results are shown in figure 10.

The first conclusion that we draw is the fact that correlated residuals indicate a mismatch between the trial function (a circle) and the data set. Ideal residuals will have a random distribution as in the earlier plots (figure 4). Interestingly enough, although the trial function does not match the data set, both the trial function and the data sets are symmetric about the origin.

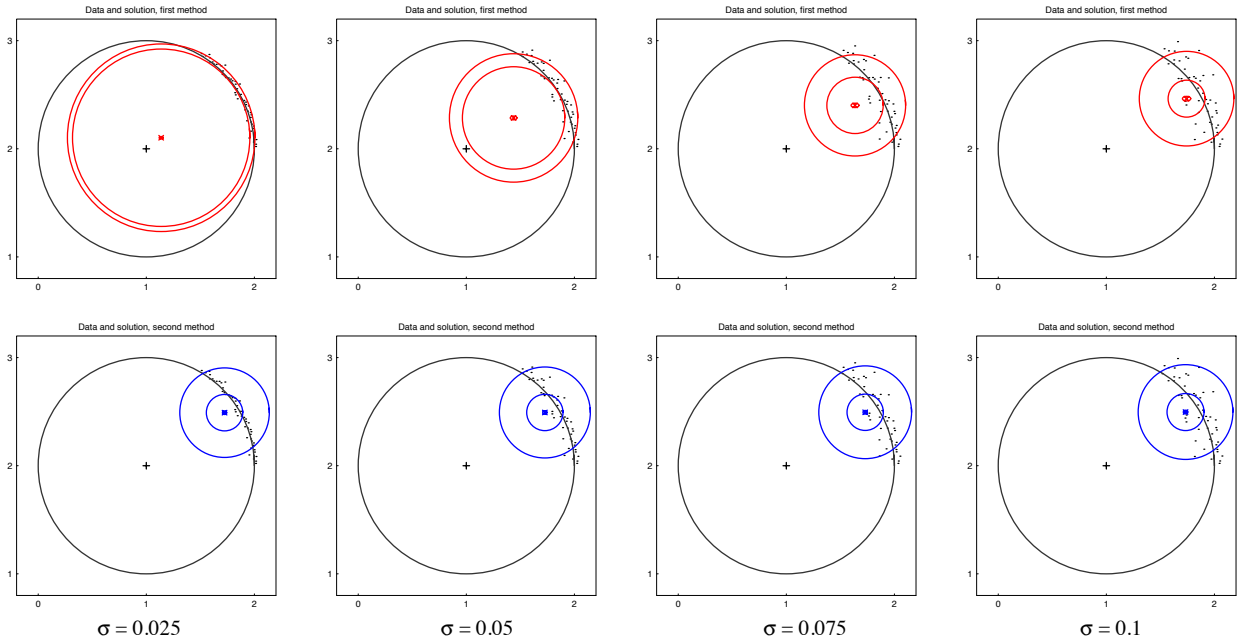

Figure 11: A series of data where only a small portion of the circle is populated. The input noise parameter σ increases as we move left to right. The results of the first method are shown in the top series with red; the second method in the bottom series with blue. The two outer circles denote $\bar{r}_m \pm \sigma_{r_m}$; the innermost circle is the uncertainty ellipse with radii σ. In this test, the first method is the clear winner since it was able to produce a reasonable answer in the low noise case.

Because of this shared symmetry, the regression returns a reliable measurement of the origin. Although in the case of the first method, there is considerably less precision in the elliptical case. However, the radius measurements did not fare so well.

For the elliptic case, we would expect a priori to have trouble defining a radius since an ellipse is defined with to radii - the semimajor and semiminor axes. In these cases, the regression returns a radius in-between the axes. The radius calculation for the square defies intuition. While on may expect the corners to be outside of the radius, we would expect to see many more points outside also. In other words, we expected a smaller circle.

4.3.2 Non-circular data

We can gain some insight by examining data that is not distributed uniformly around a circle. We will consider three cases: the first, when just some quadrant of the circle is populated; the second when two quadrants are populated; and finally, we will look a linear array.

Figure 11 shows what happens when we have a few points on one quadrant. The input noise σ takes the values 0.025, 0.05, 0.075, and 0.1 as we move from left to right. The first methods is drawn in red; the second in blue. It is apparent that the first method is a bit more robust. For the low-noise regime, it actually produces a reasonable result, whereas the second method never yields a reasonable answer with these data.

The next case involved two quadrants being populated in some balanced fashion. As seen in figure 13, the performance of the two methods was comparable in this series. The input noise was varied in the same fashion as the previous test. In this series, a slight edge is given to the second method due to the fact that the uncertainty in the origin location is higher for the first method.

The final case we will consider is a simple linear arrangement. We expect - and see - enormous fluctuations as the origin jumps above and below the data due to tiny variations in the data set. We considered a data set of 81 uniformly spaced points on the interval (1, 2) to (3, 2) and varied the noise added to the ordinate. The data and fits are shown below in figure 12. Again, we increase the noise as we move left to right.

This is a very interesting data set. The first thing that we notice is that the first method is oscillating, placing the origin above and below the data. The final two sets on the right have the same input noise and we see the first method is flipping above and below the data. The key parameter to watch here is the uncertainty in the origin location. These data reveal that the origin solution is unstable. On the other hand, the second method is very stable and we see a smaller uncertainty in the position of the origin.

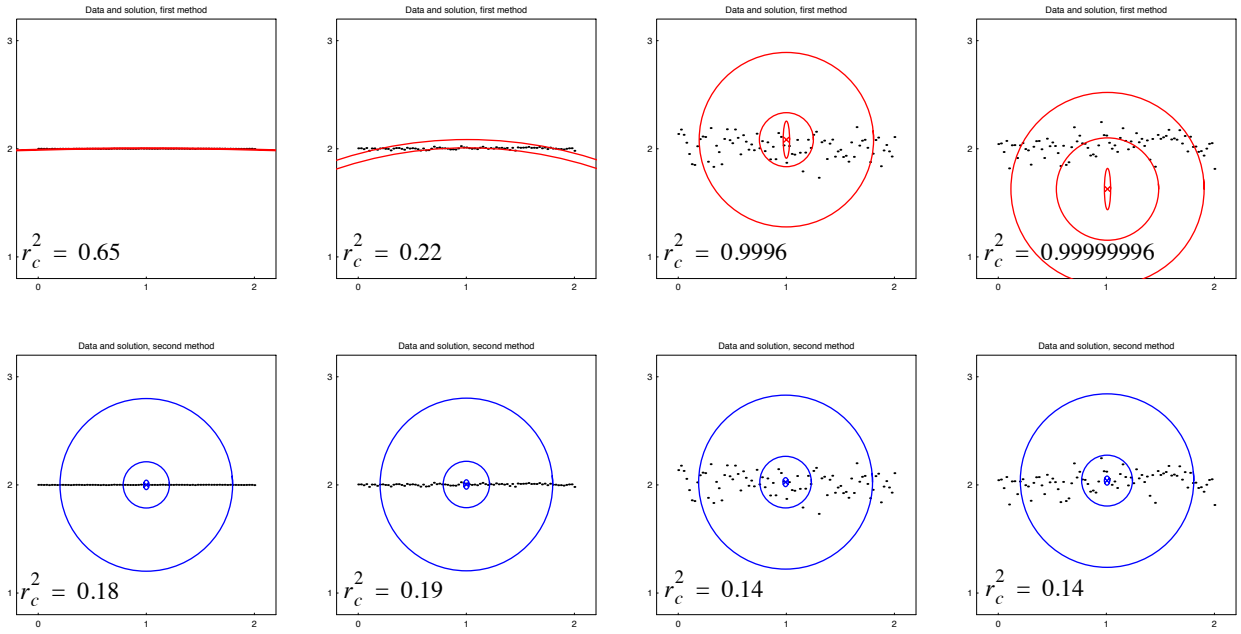

Figure 12: Trying the methods against linear data. The input noise increases as we move left to right. The noise parameter σ takes the values 0.001, 0.01, 0.1 and 0.1 respectively. The repetition of the last noise value shows how the first method solution oscillates. The results of the first method are shown in the top series with red; the second method in the bottom series with blue. The two outer circles denote $\bar{r}_m \pm \sigma_{r_m}$; the innermost circle is the uncertainty ellipse with radii σ. The first method offers oscillatory solutions; the radii vary greatly and the origin is bouncing between be over and then under the data set. Notice that the last two columns on the right have the same noise level. Small changes in the data set cause a huge change in the solution. The first method is unstable when applied to data of this form. Also, the correlation indices for the first method are a deceptive 0.9996 and 0.99999996. The second method performs well here offering a stable, slowly varying solutions as the noise varies.

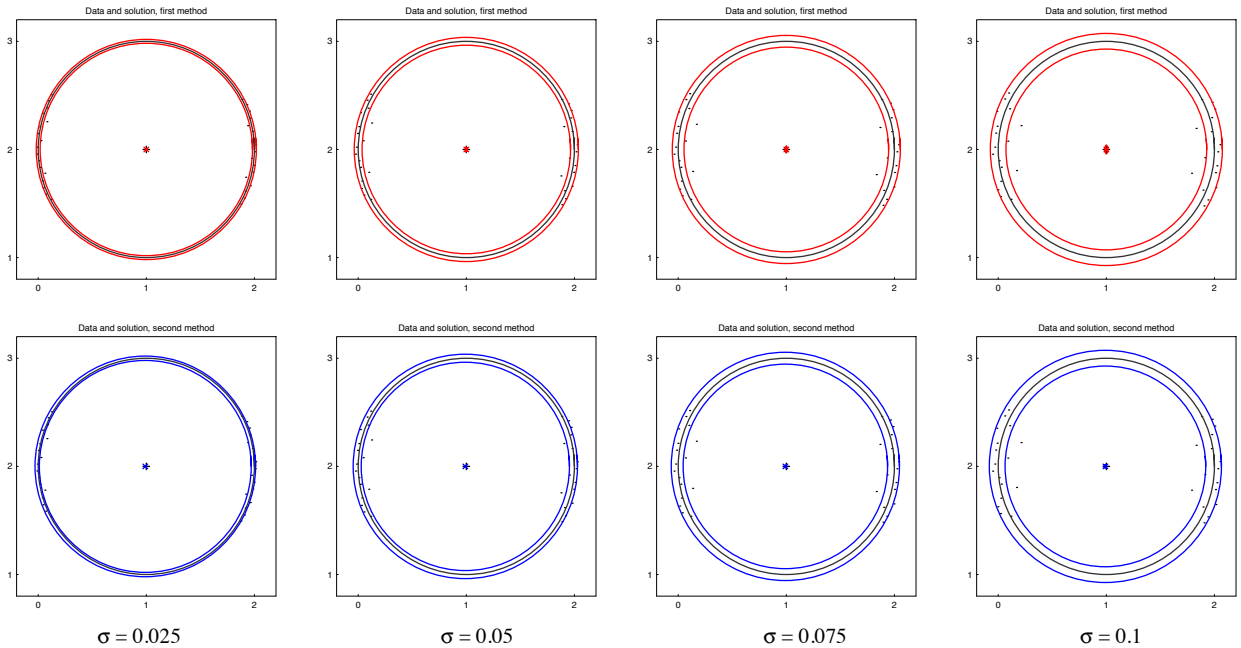

Figure 13: A series of data where the sample population is balanced. The input noise varies as in the previous figure. The results of the first method are shown in the top series with red; the second method in the bottom series with blue. The two outer circles denote $\bar{r}_m \pm \sigma_{r_m}$; the innermost circle is the uncertainty ellipse. Both methods perform quite well with the balanced data set, although the second method is slightly better due to the smaller uncertainties in the origin location.

μ	θ_μ	δr_μ	$T_\mu(\theta)^T$
1	$\pi/4$	0.004381154	$(\sqrt{2}^{-1}, \sqrt{2}^{-1})$
2	$\pi/2$	0.004972708	(0, 1)
3	$3\pi/4$	-0.002973573	$(-\sqrt{2}^{-1}, \sqrt{2}^{-1})$
4	π	0.007297957	(-1, 0)
5	$5\pi/4$	-0.018109113	$(-\sqrt{2}^{-1}, -\sqrt{2}^{-1})$
6	$3\pi/4$	0.00325291	(0, -1)
7	$7\pi/4$	0.003429889	$(\sqrt{2}^{-1}, -\sqrt{2}^{-1})$
8	2π	-0.008526847	(0, 0)

Table 5: The benchmark data set.

We close this section with an observation of the correlation index for the first method. In the two figures on the right the correlation index is 0.9996 and 0.99999996 respectively. However, it is apparent from looking at the data that there is no semblance to a circle whatsoever. Clearly, when evaluating a fit, one must look at the residuals, the uncertainties, the correlation and, if possible, the accuracy.

The second method has a necessary attribute for a quality fit: there is a slow variation and in the computed parameters as the noise increases. Notice that the radius and origin uncertainties vary slowly as the noise increases and that the origin location shows little perceptible change. Of course we do not expect to encounter data such as this, but presenting such cases helps us learn more about the method of least squares.

4.4 Benchmark

The purpose of this section is to present a simplified data set and a set of extended answers to provide a benchmark for code development. This test is rather simple and a success simply means that the code is ready for a much more extensive validation. The results are shown in full computed precision to facilitate comparisons.

If we introduce a vector form of the trigonometric functions

$$T_\mu(\theta) \equiv \begin{bmatrix} \cos\theta \\ \sin\theta \end{bmatrix}, \tag{68}$$

then we can rewrite equation 17 as

$$p_{i_\mu} = q_\mu + (\rho + \delta r_\mu) T_\mu(\theta) . \tag{69}$$

which enables one to construct the list of eight points shown in table 5.

As explained in section 3.1, this data set has an effective radius which is used to compare to the measured effective radii generated by the two methods. Here the effective radius given by equation 18 is 1.0012529108375 ± 0.004896407419878437

Before we perform the regression analysis, we need to define the points for the inverse parabolic interpolation. The lists of x and y values are $x = (0, 1, 2)$ and $y = (1, 2, 3)$. The regression results are these:

First method results (equation 37):
origin: (0.9982848521902625, 2.0003998009084345) ± (0.002992669179404519, 0.0029856534148886955)
measured effective radius: 1.001253684360645 ± 0.004733276962562515
correlation index: 0.9999108746908677

Second method results (equation 57 and 59):
origin: (0.9991006658536954, 2.0003168195979972) ± (0.002130718136874181, 0.0021282191216047473)
measured effective radius: 1.0012531376038636 ± 0.004769697179185216
correlation index: 0.9999095362878871

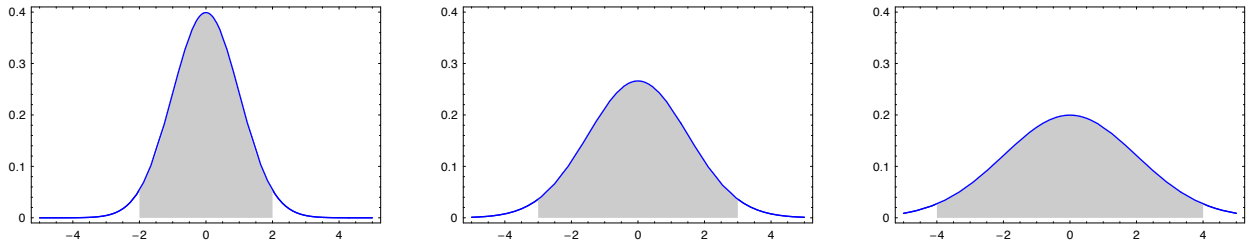

Figure 14: A look at the normal distribution. This is a plot of the function in equation 15 with μ = 0 and σ = 1, 1.5 and 2 respectively. The shadings shows the area under the curve for two standard deviations. The shaded areas under all three curves are equal. Ideally, a measurement outside of the shaded area has a 4.55% chance of belonging to the data set.

5. Data rejection

A great advantage of the least squares procedure is the valuable statistical information it offers. The quality measures on the fitting parameters are an excellent guide to evaluate the quality of the fit. This information can also be used to reject bad data points. To discuss this process, we rely upon the assumption that the errors are normally distributed.

The normal or Gaussian distribution in equation 15. The curve is normalized to unit area; this means that the area under the curve can have a physical meaning. The probability p of making a measurement whose values lies between x_1 and x_2 is

$$p = \int_{x_1}^{x_2} P(x)dx \,. \tag{70}$$

It is convenient to discuss the distribution in terms of the standard deviation, σ. In this case the likelihood that a measurement lies within one standard deviation is

$$p = \int_{-\sigma}^{\sigma} P(x)dx = 0.6827 \,, \tag{71}$$

or 68.3%. In general, the probability that a measurement lies within n standard deviations is $erf(n/\sqrt{2})$. Table 6 list the probability or likelihood for one through eight standard deviation. Another way to look at the table is to consider unity minus the likelihood. For example, if a data point were 3 standard deviations from the mean, there is a 0.27% chance that the data belongs to the measurement set.

A exclusion criteria could be to reject all measurements outside of three standard deviations. This means that, in the continuum limit, we will be using 99.7% of the data and rejecting 0.3% of the data.

Figure 15 shows how this process works. A sample data set was created. The last point was manually overwritten with a extreme outlier point. Both methods were applied to the corrupted data set. The outlier point at zero radians was almost six standard deviations away. The probability that this point belongs to the data set is roughly a few per billion, so excluding this point seems prudent. The figure shows the application of both methods first to the corrupted data set and then to the reduced data set. The results were surprising.

n	likelihood
1	0.6827
2	0.9545
3	0.9973
4	1 – 6.3 E-5
5	1 – 5.7 E-7
6	1 – 2.0 E-9

Table 6: Probability and standard deviation

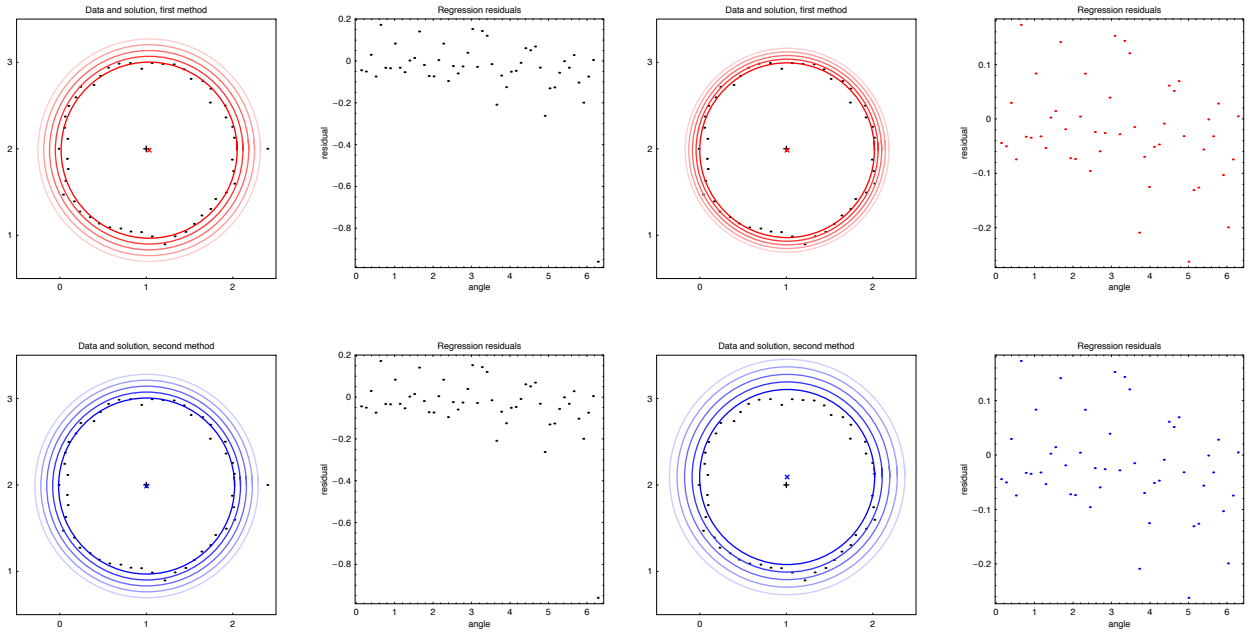

corrupt point at $\theta = 0$ *corrupt point rejected*

Figure 15: An example of data rejection. The input noise is 0.05; 50 points were generated. The two columns of the left depict a data set with an extraneous point at zero radians. The two columns on the right show the results using the data set with the extraneous point removed. For the regression results, the first circle represents $\bar{r}_m$; the next four rings demarcate one through four standard deviations. The first method, in red, behaves as expected. However the second method, in blue, has a counter-intuitive beahvior: removing the extraneous points degrades the quality of the solution.

The first method behaved as expected. When the corrupt data point was removed, the quality of all metrics improved, as shown in table 7. The precision and accuracy of the origin and radius computations showed noteworthy improvements; the correlation index also improved. A look at the regression plots reveals the origin location migrates closer to the ideal origin and the uncertainty bands become much tighter.

		full data set	reduced data set
first method	origin precision	0.015	0.009
	origin accuracy	0.023	0.012
	radius precision	0.067	0.042
	radius accuracy	-0.008	0.000
	r_c^2	0.979	0.993
second method	origin precision	0.011	0.013
	origin accuracy	0.007	0.030
	radius precision	0.069	0.087
	radius accuracy	-0.007	-0.002
	r_c^2	0.978	0.970

Table 7: Numerical results comparing full data set to reduced data set

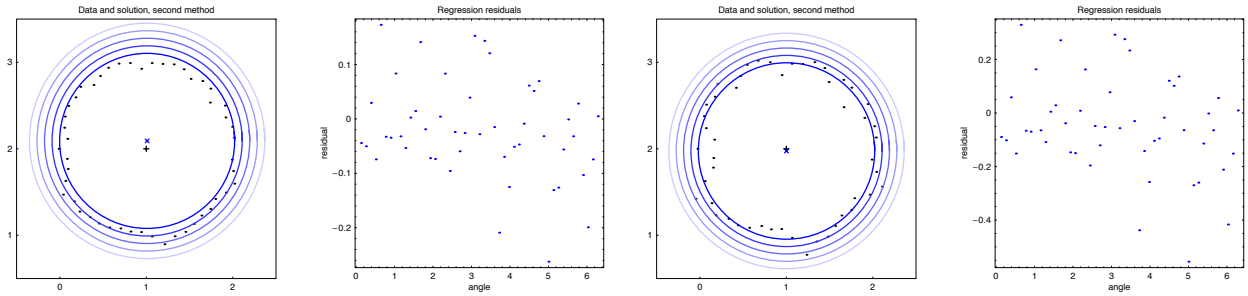

direct solution (equation 54) *iterative solution*

Figure 16: Generalizing the second method. The first two figures on the left, the direct solution, are duplicated from figure 15. The two figures on the right, the iterative solution, represent a more general form of solution to the problem posed in equation 50. This iterative solution loses the speed advantage over the first method, but the result is of higher quality as shown in table 8.

The surprise came when we looked at the data for the second method. Other than an improvement in the radius accuracy, the reduced data set was marked by clearly inferior results. The origin precision worsened slightly, the origin accuracy degraded significantly, and the radius precision worsened. An examination of the plot shows the loosened error bands. Also the correlation index showed a modest loss. Such results demanded clarification.

The source of the trouble is manifest in equation 56. As explained in the discussion following equation 50, equation 56 yields an exact answer when the merit function is quadratic. This is true when the data are uniformly sampled, as we expect the laboratory measurements to be. However, in this example, the symmetry is sacrificed to remove the corrupt datum. In this instance, equating 56 finds the minimum (the origin) at (1.00341, 1.98727). The true minimum is at (1.00721, 1.98798). Notice how this error manifests as significant vertical shift as evidenced in the figure 16.

To further resolve this issue, a data set was generated with not only radial variation, but also angular variation. Then both the direct and iterative versions of the second method were applied. The points and solutions are shown in figure 17. These results are intriguing. There is a noticeable improvement in the origin precision when going from the first method to the second method, but there is no change in the radius precision. The correlation indices are all equivalent.

The purpose of this excursion is to compare the direct and iterative formulations of the second method for asymmetric data. And we see very little difference with the exception of the accuracy degradation of the iterative formulation of the second method. It is reasonable to conclude that for this data set, the direct formulation is superior in terms of both speed and quality of result.

Unfortunately, this exercise did not resolve the unusual behavior of the second method with a uniformly distributed data set with a point removed. This phenomenon is left as an open question.

		full data set	reduced data set
second method, direct	origin precision	0.011	0.013
	origin accuracy	0.007	0.030
	radius precision	0.069	0.087
	radius accuracy	-0.007	-0.002
	r_c^2	0.978	0.970
second method, iterative	origin precision	0.011	0.007
	origin accuracy	0.016	0.007
	radius precision	0.067	0.043
	radius accuracy	-0.007	0.001
	r_c^2	0.979	0.993

Table 8: Numerical results comparing full data set to reduced data set in two implementations of the same method.

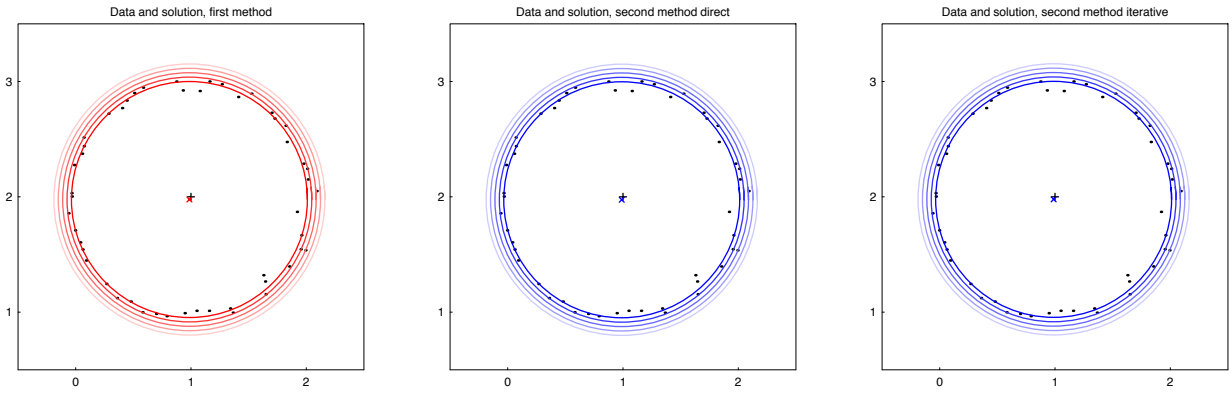

first method | *second method, direct* | *second method iterative*

origin precision:	0.008	0.005	0.005
origin accuracy:	0.018	0.017	0.016
radius precision:	0.038	0.038	0.038
radius accuracy:	6.3 E-5	6.4 E-5	7.2 E-5
correlation index:	0.995	0.995	0.995

Figure 17: A look at data with a normal noise distribution in both the radius and the angle. The purpose of this data set was to test asymmetric data sets against the first method and two formulations, direct and iterative, of the second method. In this comparison, both formulations of the second method are essentially equivalent.

6. References

1. Anton, H., *Elementary Linear Algebra* 3e, Wiley, 1981.
2. Bevington, P.R., *Data Reduction and Error Analysis for the Physical Sciences*, McGraw-Hill, 1969.
3. Press, W.H., Teukolsky, Vetterling W.T., Flannery, B.P, *Numerical Recipes in FORTRAN* 2e, Cambridge, 1992.
4. Weisstein, E.W., *CRC Concise Encyclopedia of Mathematics* on CD-ROM, Chapman & Hall/CRC, 1999.